Application of Nafion/Platinum Electrodes (Solid Polymer Electrolyte Structures) to Voltammetric Investigations of Highly Resistive Solutions

David W. DeWulf* and Allen J. Bard**

Department of Chemistry, The University of Texas, Austin, Texas 78712

ABSTRACT

Platinum electrodes on Nafion[1] 115 membranes, designated Pt/Naf and prepared by an electroless plating method ($PtCl_6^{2-}$ with hydrazine), were used for voltammetric investigations. Scanning electron microscopy (SEM) of these electrodes showed the Pt electrode surface to have the continuous, yet porous, structure necessary for both electronic conduction to the Pt particles and ionic conduction through the membrane/electrode/solution interface. These electrodes were used in the configuration S/Pt/Naf/H_2O + electrolyte, where the counter and reference electrodes were in the aqueous electrolyte solution and the substance of interest was dissolved in solvent, S. Cyclic voltammetry was used to characterize the behavior of several substrates in H_2O, MeCN, THF, and toluene. Tetracyanoquinodimethane (TCNQ) in acetonitrile (MeCN), tetrahydrofuran (THF), and toluene and benzoquinone (BQ) in THF and toluene could be reduced to anion radicals in the absence of added supporting electrolyte. In THF and toluene, the formation of the radical anion of BQ and TCNQ often involved ion pair formation with alkali metal ion and precipitation. The reduction of TCNQ in toluene in the presence of Na^+ ions resulted in the formation of the electronically conducting salts, Na^+TCNQ^-.

This paper describes the construction of Pt electrodes, based on solid polymer electrolyte (SPE) technology, that can be employed for voltammetric measurements and their application to studies with several solvent systems, including some very resistive ones that contain no or low amounts of added supporting electrolyte. SPE techniques involve the use of an ion exchange membrane (usually Nafion[1]) with porous contacting electrodes for the construction of electrochemical devices in which ionic migration to maintain charge neutrality occurs within the membrane. SPE technology was first applied to fuel cells (1) and later to water electrolyzers (2) and electrochemical oxygen separators (3). Our goal was to utilize these SPE electrodes in a voltammetric mode to help establish appropriate conditions for bulk electrolysis and for analysis. In this way such SPE electrodes could be used to complement ultramicroelectrodes (4, 5) in the electrochemical characterization of systems in resistive media. We also were interested in obtaining a better understanding of the operation and structure of the voltammetric SPE electrode.

Recently platinum electrodes bonded to, or in contact with, solid polymer electrolyte membranes have been proposed for electrochemical synthesis (6-8). The principle is illustrated in Fig. 1. The membrane/electrode separates the working solution, which contains the solvent and substrate of interest, and the counter solution with the solvent (*e.g.*, water) and supporting electrolyte, along with the auxiliary and reference electrodes. The membrane is an inert, ion exchange polymer (*e.g.*, Nafion) with metal deposited onto the face that contacts the working solution. When the metal electrode is held at an appropriate potential, the substrate in the working solution is reduced or oxidized, coupled with an ionic migration through the membrane to maintain electroneutrality. Concurrently, some species in the counter solution react at the auxiliary electrode. In this way, electrolyses can be carried out in highly resistive solvents without the need for supporting electrolyte. Using this method, Ogumi and co-workers reported the hydrogenation of olefins in n-hexane under constant current conditions, but at low current efficiencies (11-44%) and high potentials (4-8V) (6a). However, most of the previous studies have involved bulk electrolysis with protic working solvents, such as methanol (7a, b), ethanol (6a, c, 7c), acetic acid (6b), or aqueous mixtures (6c, 8), as the working compartment solvents and were concerned with the application of the SPE technique to electro-organic synthesis.

Experimental

Platinum-bonded membranes were prepared by a previously published electroless plating method (9). The solid polymer electrolyte (SPE) membrane material was Nafion 115 (equivalent weight = 1100, 5 mil thickness; E.I. du Pont de Nemours and Company, Incorporated, Wilmington, Delaware), which was cleaned by boiling in concentrated HNO_3 for 1h and then in milli-Q reagent grade water (Continental Water Systems, El Paso, Texas) for 1h. The Nafion was clamped between two half-cells, with one compartment containing 0.2*M* hydrazine (Fisher Scientific, Fair Lawn, New Jersey) in an aqueous alkaline solution (*p*H = 13) and the other compartment containing 0.02*M* $PtCl_6^{2-}$ in an HCl solution (*p*H = 2) (Fig. 2). The cell was allowed to stand for 48-72h with occasional stirring to release bubbles trapped on the membrane surface, during which time Pt metal formed on the $PtCl_6^{2-}$ side. The membrane was removed when the platinized side had a metallic appearance. The membranes were converted to the appropriate cationic forms by boiling in 1*M* HCl, then treated with corresponding base to yield the Li^+, Na^+, and K^+ forms.

Benzoquinone (BQ) (Aldrich Chemical Company, Milwaukee, Wisconsin) was sublimed under vacuum at room temperature, and tetracyanoquinodimethane (TCNQ) (Sigma Chemical Company, St. Louis, Missouri) was recrystallized three times from ethyl acetate (Fisher Scientific) (10). Other redox couples, $K_4Fe(CN)_6$, $Ru(NH_3)_6Cl_2$, and hydroquinone (Aldrich), were used as received. Supporting electrolytes, K_2SO_4, Na_2SO_4, H_2SO_4, KCl, NaCl, LiCl (Fisher Scientific) and tetramethylammonium chloride (TMACl), $LiClO_4$ (Aldrich), as well as solvents acetonitrile (MeCN), tetrahydrofuran (THF), and toluene (Fisher Scientific), were also used without further purification. Be-

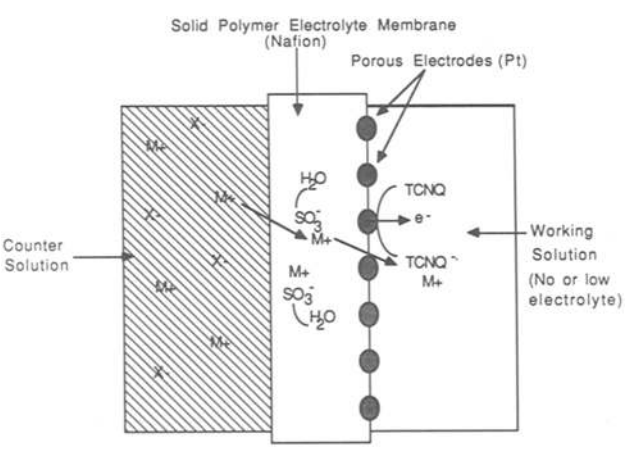

Fig. 1. Schematic diagram of porous metal electrode supported on a solid polymer electrolyte membrane for electrochemistry in a resistive solution without added supporting electrolyte.

*Electrochemical Society Student Member.
**Electrochemical Society Life Member.
[1]Nafion is a registered trademark of E.I. du Pont de Nemours and Company, Incorporated.

Downloaded 02 Feb 2009 to 146.6.143.190. Redistribution subject to ECS license or copyright; see http://www.ecsdl.org/terms_use.jsp

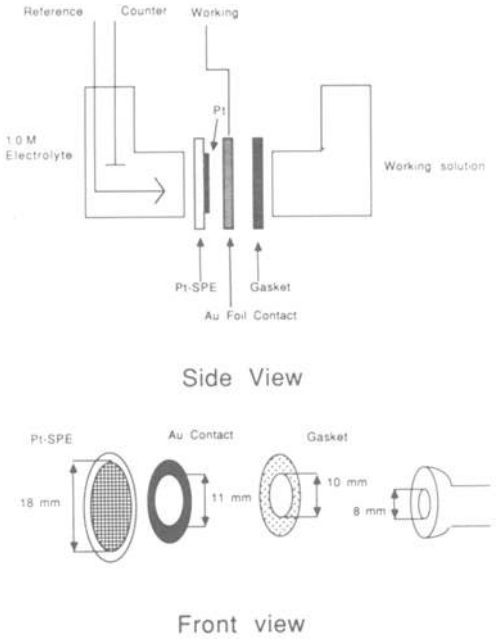

Fig. 2. Electrochemical cell configuration

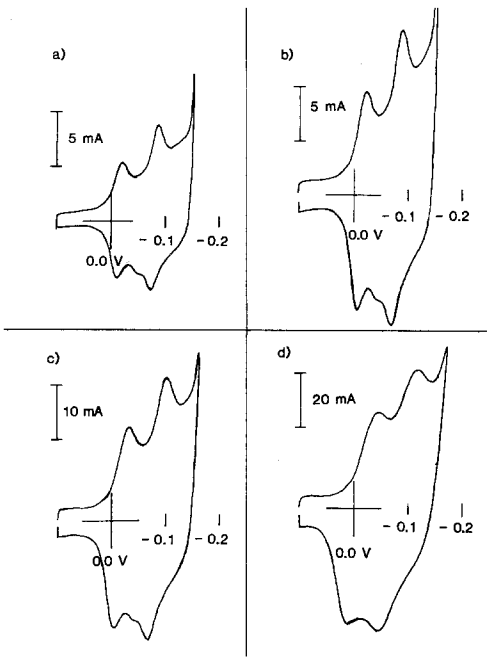

Fig. 3. Cyclic voltammograms of hydrogen adsorption waves at a platinum-SPE electrode in 1M H_2SO_4. Electrode geometric area = 0.50 cm^2, all potentials in V vs. SCE: (a) 5; (b) 10; (c) 20; (d) 50 mV/s.

cause the counter solution in all cases was an aqueous one and since small amounts of water were expected to permeate through the Nafion film during the operation, we did not think it necessary to remove water from these solvents.

The two-compartment cell used for all experiments is shown schematically in Fig. 2. Between the two half-cells were clamped the platinum-solid polymer electrolyte membrane (Pt-Naf) electrode, a Au ring foil (0.025 mm, 99.99+%, Alfa Products, Danvers, Massachusetts) as an electrical contact, and a Neoprene (for aqueous experiments) or Teflon[2] (for nonaqueous experiments) gasket that defined the projected area of the electrode that was exposed to the working solution. For the larger electrode (L), the gasket hole diameter was about 8 mm, while for the small electrode, (S), it was about 1.5 mm. The platinized side of the membrane faced the working solution, which contained redox couple but no added electrolyte. The unplatinized side faced the counter solution, which contained an aqueous solution with supporting electrolyte along with the reference electrode and a platinum gauze counterelectrode. Cyclic voltammograms were obtained with a PAR Model 173 potentiostat/galvanostat, a PAR Model 174 universal programmer, and were recorded with a Norland Model 2000 data acquisition and management system (Norland Instruments, Fort Atkinson, Wisconsin). Chronocoulometry employed the same PAR programmer/potentiostat apparatus, with an additional PAR Model 179 digital coulometer, and was recorded on a Houston Instruments Model 2000 X-Y recorder (Houston Instruments, Austin, Texas). AC conductance measurements were made with a Yellow Springs Instrument Model 321 conductance meter (Yellow Springs, Ohio), which operates at a frequency of 1 kHz. The scanning electron microscope (SEM) was a JEOL JSM-35C (Japan Electric Optical Laboratories, Limited, Tokyo) and the spectrophotometer was a Hewlett-Packard Model 8450 (Hewlett-Packard, Palo Alto, California).

Results and Discussion

Large electrode electrochemical and microscopic characterization.—The cyclic voltammetric behavior of Pt-SPE electrodes in 1M H_2SO_4 solution followed the well-defined pattern observed with larger area electrodes (3-5 cm^2) by other investigators (8b). Determination of the actual area of the electrode was performed by integration of the hydrogen adsorption peaks at sweep rates of 5-50 mV/s (Fig. 3) (12, 13). With the assumption that complete coverage of hydrogen on platinum corresponds to 210 $\mu C/cm^2$ (14), we calculated an area of 108 (± 5) cm^2. The geometric area measured 0.50 cm^2, yielding a roughness factor of *ca.* 200, similar to previously reported values (8). Chronocoulometry of 10 m*M* $Fe(CN)_6^{3-}$ in 1.0*M* KCl solution at times of 0.7-4.2s yielded linear Q *vs.* $t^{1/2}$ plots. The area determined from the slopes of these lines, with a diffusion coefficient, D, for $Fe(CN)_6^{3-} = 7.63 \times 10^{-6}$ cm^2/s, was 0.53 (± 0.03) cm^2, which agrees well with the geometric area. Since the chronocoulometric data yield area measurements that correspond to the geometric area, within the time of the experiment, the diffusion layer had grown beyond the surface roughness. Since the diffusion layer thickness, δ, at time, t, is $\delta \cong \sqrt{2Dt}$, the average surface asperity from these measurements is less than *ca.* 35 μm.

Scanning electron microscopy (SEM) of the electrode face (Fig. 4a) showed that the deposited platinum, as determined by x-ray fluorescence, was distributed as islands (*ca.* 10-50 μm) separated by pores of μm dimensions, which are necessary for ion transport. A pore is shown at higher magnification in Fig. 4b. Figure 4c is a cross-sectional view of the Pt-SPE electrode, with Pt side facing right; the "back" (left) side has no platinum deposited on its surface. The average surface roughness (peak-to-trough height) is on the order of 10-15 μm, while the largest roughness, *ca.* 25-30 μm, is in good agreement with the chronocoulometric estimation. Also evident is the porous and channeled nature of the deposited platinum. Previous investigators had reported that only one face of the membrane was metallized during the fabrication process because of electrostatic exclusion of anionic $PtCl_6^{2-}$ from the anionic SPE membrane (8c). However, we found many platinum nodules deep inside the polymer membrane (80-90 μm from the Pt face). Hydroxyl anions can diffuse through Nafion to a limited extent (15). By analogy, $PtCl_6^{2-}$ must diffuse through Nafion as well to be reduced by the hydrazine, which is diffusing in the opposite direction. These nodules probably do not contribute to the working electrode area and exist as isolated islands in a sea of Nafion, as shown in Fig. 4d. If these contribute to the area, a roughness factor much larger than 200 would be expected. Figure 4e is a view *ca.* 45° from the plane normal to the face of the electrode, showing both facial and interior structure. This view suggests that the active surface Pt electrode structure is shallow (10-20 μm) and that much of the structure appearing near the facial region in the cross-sectional view arises from crushing of the surface Pt when the sample is cut.

[2]Teflon is a registered trademark of E.I. du Pont de Nemours and Company, Incorporated.

Downloaded 02 Feb 2009 to 146.6.143.190. Redistribution subject to ECS license or copyright; see http://www.ecsdl.org/terms_use.jsp

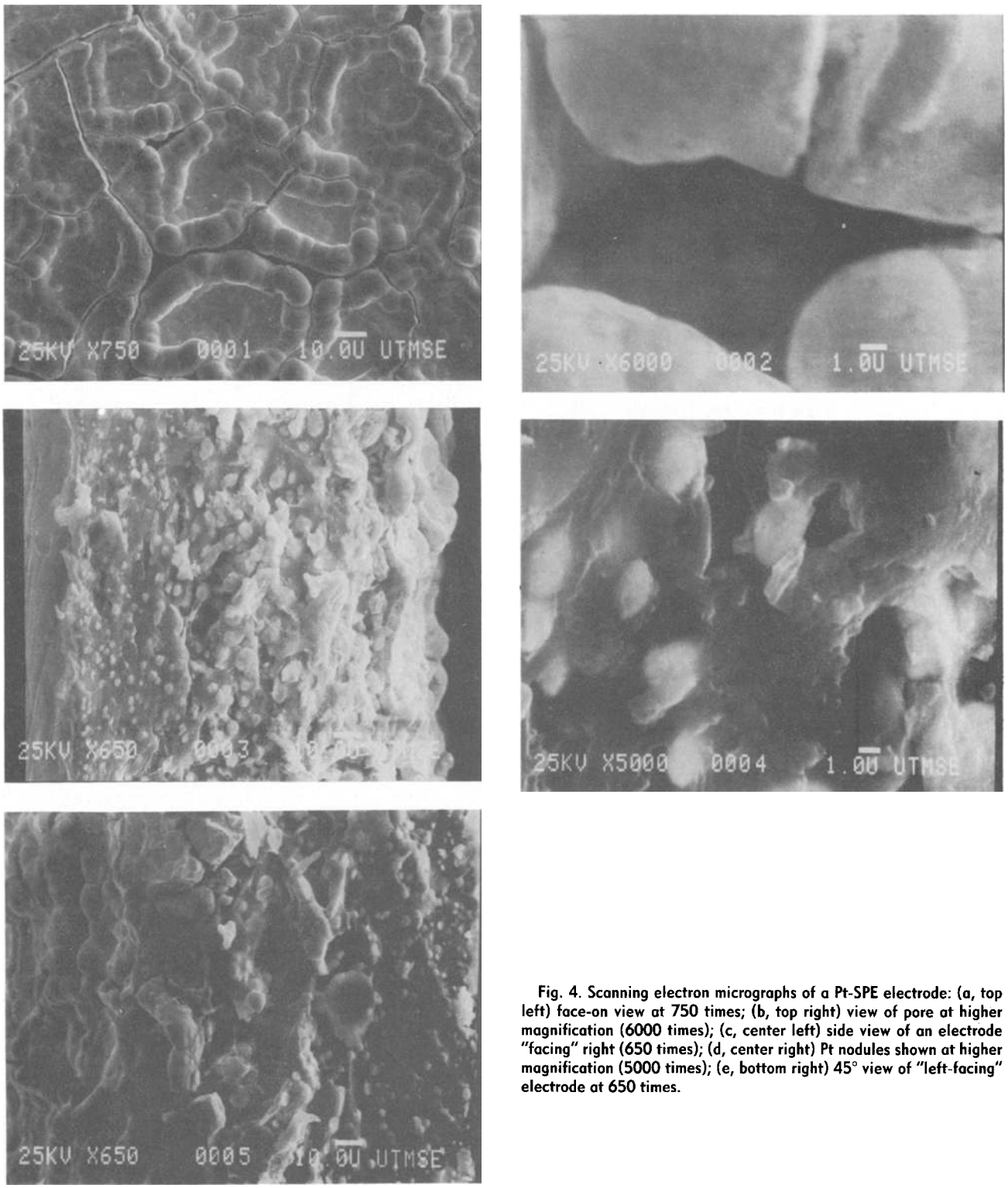

Fig. 4. Scanning electron micrographs of a Pt-SPE electrode: (a, top left) face-on view at 750 times; (b, top right) view of pore at higher magnification (6000 times); (c, center left) side view of an electrode "facing" right (650 times); (d, center right) Pt nodules shown at higher magnification (5000 times); (e, bottom right) 45° view of "left-facing" electrode at 650 times.

The diffusion coefficient of $PtCl_6^{2-}$ in Nafion was estimated by measuring the flux through a membrane clamped between two half-cells, one containing 0.040*M* $PtCl_6^{2-}$ (*p*H = 1), and the other 1*M* HCl or 1*M* $NaHSO_4$. The concentration of $PtCl_6^{2-}$ in the HCl (or $NaHSO_4$) compartment was monitored spectrophotometrically at 260 nm (17) until it reached $4.0 \times 10^{-5}M$. Under these conditions, the following boundary conditions hold

$$C_{PtCl_6^{2-}} = 0 \text{ at } 0 < x < d; \text{ for } t < 0$$

$$C_{PtCl_6^{2-}} = 0 \text{ at } x = 0; \text{ for } t > 0$$

$$C_{PtCl_6^{2-}} = C_o \text{ at } x = d; \text{ for } t > 0$$

and the solution for steady-state flux under linear diffusion becomes

$$J = DKC_o/d \quad [1]$$

where K is the partition coefficient of $PtCl_6^{2-}$ between the aqueous solution and the Nafion membrane, d is the membrane thickness and D, the diffusion coefficient of $PtCl_6^{2-}$ in the membrane. Figure 5 shows a plot of moles $PtCl_6^{2-}$ transported per unit area of membrane *vs.* time. The linear portion represents steady-state conditions, and the slope of the line is the steady-state flux, J. The partition coefficient for $PtCl_6^{2-}$ between Nafion and aqueous solution was also measured spectrophotometrically after soaking a membrane in 0.040*M* $PtCl_6^{2-}$ for 72h. The absorbance at a 0.13 mm thick Nafion membrane was 0.136, while that of the $PtCl_6^{2-}$ soaked membrane was 0.642. If the molar ab-

Downloaded 02 Feb 2009 to 146.6.143.190. Redistribution subject to ECS license or copyright; see http://www.ecsdl.org/terms_use.jsp

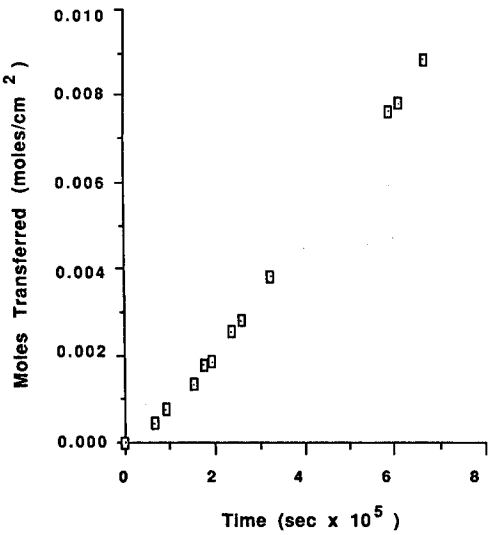

Fig. 5. Amount of $PtCl_6^{2-}$ diffusing through Nafion 115 per unit area vs. time. Slope of linear portion = 1.2×10^{-12} mol cm^{-2} s^{-1}.

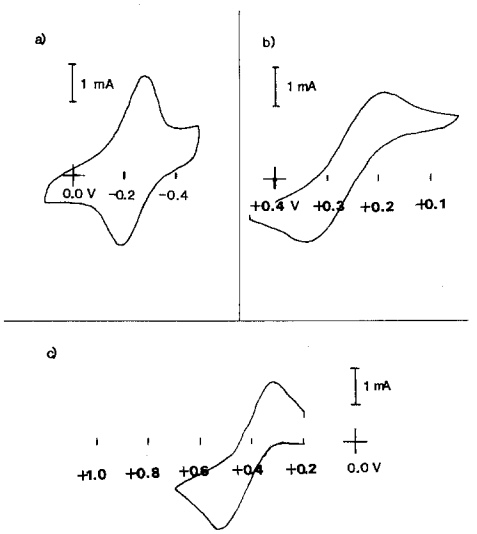

Fig. 6. Cyclic voltammograms of aqueous redox couples at a 0.50 cm^2 Pt-SPE. K^+ form Nafion was used for all experiments, and all potentials are measured in V vs. SCE and all at 10 mV/s: (a) 10 mM $Ru(NH_3)_6Cl_2$, (b) 10 mM $K_3Fe(CN)_6$, (c) 5 mM HQ.

sorptivity of $PtCl_6^{2-}$ in the Nafion is taken as the same value as that in water, 27,000 at 260 nm (16), the equilibrium concentration is $1.5 \times 10^{-3}M$; the partition coefficient, $K = [PtCl_6^{2-}]_{Naf}/[PtCl_6^{2-}]_{aq}$, is 0.037. The diffusion coefficient (D) calculated from these data is 1.0×10^{-8} cm^2/s, similar to previously reported values for D of chloride and iodide ions in Nafion 125 membranes (17). The diffusion coefficient was independent of the presence of chloride ion. Assuming that the rate-limiting step for $PtCl_6^{2-}$ transport is not transport across the membrane/solution interface, but diffusion in the membrane, we calculate that $PtCl_6^{2-}$ will diffuse 90 μm into the Nafion membrane in 1h, much less than the total time (48-72h) for electrode fabrication.

A similar morphology was observed by Mazur and Reich while studying the electrochemical deposition of metal interlayers in a polymer film (18). Qualitatively, the data can be interpreted as follows. Given that the reduction of $PtCl_6^{2-}$ to Pt° by hydrazine is exoergic by almost 2 eV (19a), the rate of Pt production is probably mass transport limited. At first, the homogeneous reaction between the reductant, hydrazine, and the metal ion, $PtCl_6^{2-}$, forms small Pt nuclei. The next stage involves growth of the nuclei to form polyatomic clusters and independent microparticles. As the particles grow, the probability of a diffusing species encountering a particle increases. In addition, these particles may function as bipolar electrodes, accepting electrons (from reductant) at one surface and metal ions at another. The spherical shape suggests that the growth process is transport-limited, since there is no preference for growth along any particular crystallographic axis. The size distribution reflects the concentration gradient of the less permeative reagent, $PtCl_6^{2-}$. Mazur and Reich also observed that metal particles are only formed early in the deposition process, during a transient regime, and concluded that the steady-state process is bulk metal deposition.

The deposition process has recently been modeled by Manring (20). The equation that approximately describes the relative position of the deposited metal layer as a function of reactant diffusivities and concentrations is given as

$$x/d = D_rK_r[R]/(D_rK_r[R] + D_mK_m[M]) \quad [2]$$

where d is the thickness of the membrane; x is the distance of the deposited metal layer from the reductant side of the membrane; D_r, K_r, and $[R]$ are the diffusion coefficient, the partition coefficient, and the concentration of reductant, respectively, and D_m, K_m and $[M]$ are the diffusion coefficient, partition coefficient, and concentration of metal ion, respectively. Although D_r and K_r are unknown for N_2H_4, the permeability, P_r, of uncharged organic molecules (where $P_r = D_rK_r$), is of the order of 2×10^{-6} cm^2/s (21) (approximately four orders of magnitude larger than that of $PtCl_6^{2-}$). With this value and the previously estimated values for D_m and K_m, Eq. [2] yields a value of $x/d \sim 1$ under the conditions used in the preparation of the electrodes.

Cyclic voltammetry at large electrodes.—As a preliminary test of the system, cyclic voltammograms (CV) of several well-behaved aqueous redox couples in Milli-Q water (resistivity *ca.* $10^7\Omega$) were obtained without added electrolyte. Anionic, cationic, and neutral species [reduction of $Fe(CN)_6^{3-}$ and $Ru(NH_3)_6^{3+}$, and oxidation of hydroquinone (HQ) to benzoquinone (BQ), respectively] were used at a scan rate, v, of 10 mV/s. Reversible peak splittings, ΔE_p, (60 mV) were observed for 10 mM solutions of $Ru(NH_3)_6^{2+}$ and $Fe(CN)_6^{3-}$, indicating that no charge-specific interactions take place between ion-exchange polymer and substrate. Since the cathodic peak heights ($i_{p,c}$) of these two species at the same concentration and v, corrected for the rather large capacitive background current (see Fig. 6b), where the same, the species undergoing electron transfer is in solution rather than within the Nafion phase. Moreover, the diffusion coefficients of ionic species in Nafion are four to five orders of magnitude less than those in solution (22), predicting much smaller peak currents for polymer-bound species. The peak heights found correspond to those expected for a 0.5 cm^2 Pt electrode with a D of 10^{-5}-10^{-6} cm^2/s. At larger v, the peak currents and ΔE_p increased, although $i_{p,c}/v^{1/2}$ and $i_{p,c}/i_{p,a}$ values remained constant. These large area electrodes showed large capacitive currents (*ca.* 1-2 mA at v = 10 mV/s) and large faradaic currents during the potential sweeps. As a result, even small resistances (100-200Ω) between the working and reference electrodes created large iR drops. For this reason, smaller area electrodes (projected area = 1.98×10^{-2} cm^2) to give smaller background and faradaic currents and smaller iR-drops, were investigated.

Cyclic voltammetry at small electrodes in THF and MeCN.—Small electrodes were of similar construction to large electrodes with proportionally smaller diameter cells and gaskets. Their approximate geometric area measured 2×10^{-2} cm^2. Small electrodes were also tested with aqueous redox couples; these showed CV more closely approaching reversible behavior in the highly resistive solvents. Cyclic voltammetry at a Pt/Naf electrode of TCNQ in acetonitrile (MeCN) with no added supporting electrolyte is shown in Fig. 7; typical data are shown in Table I. TCNQ exhibits reversible waves in water (23) and MeCN (24) at a Pt electrode. At the Pt-SPE electrode in MeCN, with a TCNQ concentration of 10 mM, large peak splittings (100 mV) were found at slow scan rates (10 mV/s). The peak splittings increased with increasing v (*i.e.*, increasing $i_{p,c}$), while peak current ratios ($i_{p,a}/i_{p,c}$) were unity; $i_{p,c}/v^{1/2}$-values and the mean of the cathodic and anodic peak potentials, ($E_{p,c}$ and $E_{p,a}$), denoted E_m, were constant. Plots of ΔE_p vs.

Downloaded 02 Feb 2009 to 146.6.143.190. Redistribution subject to ECS license or copyright; see http://www.ecsdl.org/terms_use.jsp

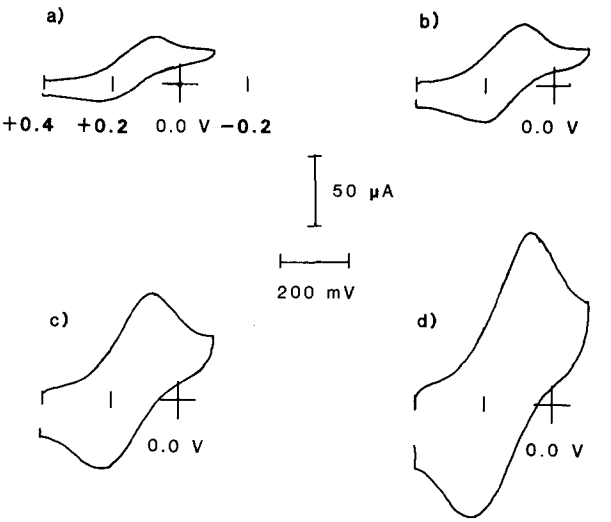

Fig. 7. Cyclic voltammograms of 10 mM TCNQ in MeCN at a 1.98×10^{-2} cm² Pt-SPE electrode in the absence of added supporting electrolyte. K^+ Nafion, all potentials *V vs.* Ag/AgCl: (a) 10, (b) 20, (c) 50, (d) 100 mV/s.

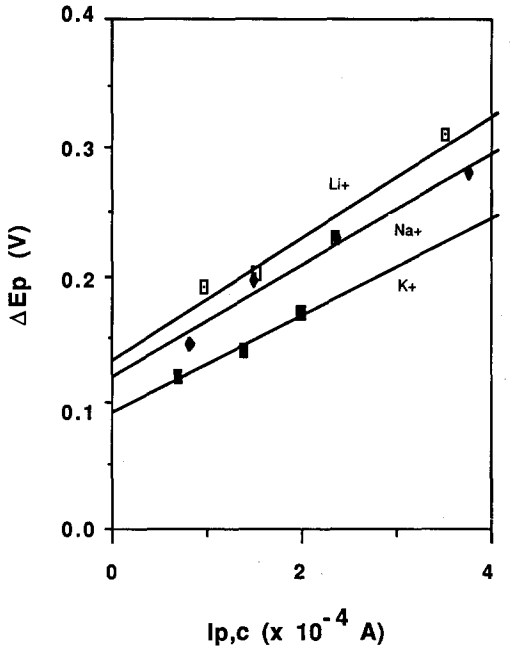

Fig. 8. Cation dependence of cyclic voltammetric behavior of TCNQ in MeCN: Li^+ Nafion, slope = 956Ω, intercept = 133 mV; Na^+ Nafion, slope = 898Ω, intercept = 116 mV; K^+ Nafion, slope = 766Ω, intercept = 91 mV.

$i_{p,c}$ shown in Fig. 8, exhibit reasonable linearity. The intercepts, ΔE_p at the limit of zero current, however, were greater than 60 mV, suggesting that simple uncompensated resistance is not the only source of the large ΔE_p-values. The intercepts follow a cation dependence of: $Li^+ > Na^+ > K^+$. If the slopes of the lines are considered as "effective resistances," values of *ca.* 400-500Ω are found. These effective resistances also show a cation dependence, with the trend $Li^+ > Na^+ > K^+$.

There are several possible processes that could provide the kinetic limitations that produce the effective resistance: ion flow through the membrane, Pt film resistance, contact resistance, slow interfacial electron or ion transfer. We feel, based on the results and discussion below, that the major contributor is cation transfer from the Nafion to the MeCN at the MeCN/Nafion/Pt three-phase interface.

Kita and co-workers calculated the radial resistance across the Pt face of a Pt-SPE electrode of geometric area 3.14 cm² (2 cm diam) as less than 0.1Ω (26). Our own ac conductance and dc resistance measurements indicate a resistance across a 2 cm Pt face of less than 0.5Ω. The resistance between the working and reference electrode leads, as measured by an ac conductance bridge at 1 kHz, was 80Ω. This measurement includes the resistances of the lead, contact, and membrane, and a small contribution from the aqueous solution between the membrane and reference electrode. Scibona and co-workers investigated the effect of electrolyte on Nafion membrane resistance under high dc current conditions. They found that membrane resistance follows the series: $Li^+ < Na^+ < K^+$ (26) (opposite to the trend in effective resistance we found). These results indicate that the effective resistance is probably not due to radial resistance across the Pt face or limited ion transport through the SPE membrane. The electron transfer reaction occurs at the three-phase MeCN/Nafion/Pt interface and involves transfer of an electron from the Pt to TCNQ with the simultaneous transfer of an alkali metal cation from the Nafion to the MeCN phase. The electron transfer reaction at the Pt/TCNQ, MeCN is known to be rapid (24), so that interfacial ion transfer may be the kinetically slow step. Scibona *et al.* also reported that the hydration number for the cations follow the series $Li^+ > Na^+ > K^+$ (26). Smaller ions of higher charge density show greater hydration numbers and would require greater activation energies for dehydration and subsequent resolvation by the less polar media (27). Therefore, in the case of overall kinetics limited by counterion transport, the expected behavior in working resistance would be: $Li^+ > Na^+ > K^+$, as observed.

In THF, a solvent of higher resistivity and lower polarity, TCNQ shows similar behavior (Fig. 9). Data are collected in Table II. The ΔE_p *vs.* i_p data for TCNQ in THF are equivalent to an effective resistance of 1250Ω, while conductance measurements yielded a reference-to-working electrode resistance of 120Ω. Unlike MeCN, little or no dependence of the peak splitting on the cation was observed for THF. The lack of this dependence in THF may be due to its greater donicity, that is, its ability to solvate cations (23); the donicity number for THF is 20 compared to 14 for MeCN (28). However, the values of the observed resistances are higher in THF than in MeCN, since THF has a di-

Table I. Cyclic voltammetric results for TCNQ in MeCN at the Pt-SPE electrode[a]

Ion in Nafion	ν (mV/s)	$E_{p,c}$ (mV *vs.* Ag/AgCl)	$E_{p,a}$	ΔE_p (mV)	E_m[b]	$i_{p,c}$ (μA)	$i_{p,a}$ (μA)	$i_{p,c}/i_{p,a}$	$i_p/\nu^{1/2}$ (μA-s$^{1/2}$/mV$^{1/2}$)
Li^+	20	+70	+260	190	+165	48	40	1.2	11
	50	+50	+250	200	+150	76	75	1.0	11
	100	+20	+250	230	+135	118	130	0.9	12
	200	−30	+280	310	+125	175	170	1.0	12
Na^+	20	+85	+230	145	+158	41	36	1.1	9
	50	+60	+260	195	+155	75	76	1.0	11
	100	+30	+260	230	+145	119	119	1.0	12
	200	+00	+280	280	+140	188	202	0.9	13
K^+	20	+95	+215	120	+155	35	35	1.0	8
	50	+85	+225	140	+155	69	70	1.0	10
	100	+65	+235	170	+150	100	103	1.0	10

[a]Working solution: TCNQ concentration, 10 m*M*; counter solution, 1.0*M* Li, Na, or KCl. Electrode area, 2.0×10^{-2} cm².
[b]$E_m = (E_{p,c} + E_{p,a})/2$ mV *vs.* Ag/AgCl.

Downloaded 02 Feb 2009 to 146.6.143.190. Redistribution subject to ECS license or copyright; see http://www.ecsdl.org/terms_use.jsp

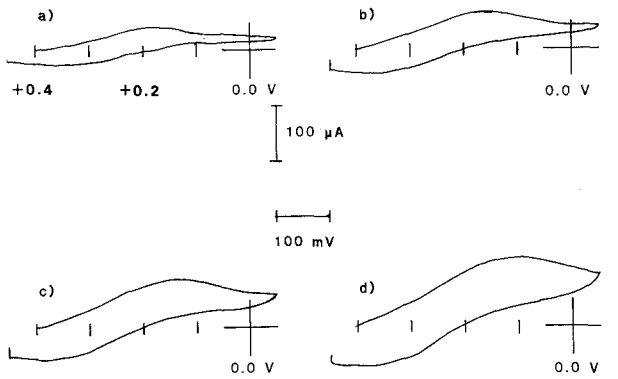

Fig. 9. Cyclic voltammetry of 10 mM TCNQ in THF at 1.98 × 10^{-2} cm^2 Pt-SPE electrode in the absence of added supporting electrolyte. Li^+ Nafion, all potentials in *V* vs. Ag/AgCl: (a) 20, (b) 50, (c) 100, (d) 200 mV/s.

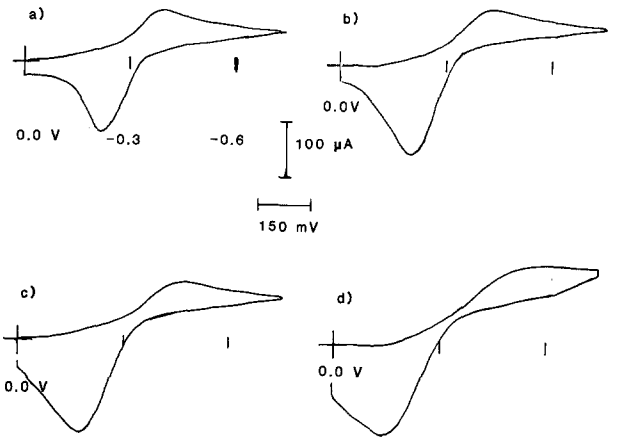

Fig. 10. Cyclic voltammetry of 10 mM BQ in THF at a 1.98 × 10^{-2} cm^2 Pt-SPE electrode in the absence of added supporting electrolyte. Na^+ Nafion, all potentials in *V* vs. Ag/AgCl: (a) 20, (b) 50, (c) 100, (d) 200 mV/s.

electric constant of 7.95, compared to that of MeCN, 38.0 (28).

Benzoquinone (BQ) was also used to test the system, since its electrochemical behavior is sensitive to the nature of the solvent environment. In water, BQ is reduced to hydroquinone (HQ) by a two-electron process at +0.502V *vs.* Ag/AgCl (19a). In aprotic solvents, such as MeCN, BQ is reduced to the anion radical by a one-electron process near −0.5V *vs.* Ag/AgCl (19a). Therefore, if the peak currents indicate a one-electron transfer, the electron transfer probably occurs in a nonaqueous environment. However, if a contribution from a two-electron process is observed, protonation effects from water contained in the Nafion membrane is suggested. Since aqueous reduction would involve protonation, the reduction potential (of the aqueous two-electron process) would allow a calculation of the pH of this aqueous environment from the measured potential.

The cyclic voltammetric behavior of BQ in THF in the absence of supporting electrolyte is shown in Fig. 10. The reduction wave appears to be diffusion controlled with an $E_{p,c}$ *ca.* −0.4 to −0.5V *vs.* Ag/AgCl (dependent on scan rate). Peak currents were essentially the same as those of known one-electron couples [$Ru(NH_3)_6^{2+/3+}$, $Fe(CN)_6^{3-/4-}$, $TCNQ^{o/-}$] at equal concentrations at the same electrode. They also agree with calculated values for $n = 1$, assuming $D = 10^{-5}$ cm^2/s and a reversible electron transfer (19b). The anodic wave was nearly parabolic in shape with peak current values 30-50% greater than $i_{p,c}$. This symmetric wave form is characteristic of thin-layer electrochemical systems (19c) and is probably caused by precipitation of the reduction product at the electrode. Although peak current ratios remained almost constant, E_m-values shifted with scan rate.

Cyclic voltammetry in toluene.—Figure 11 shows the cyclic voltammetric behavior of BQ in toluene in the absence of supporting electrolyte. The wave shapes are similar to those observed in THF. The anodic wave again shows the parabolic shape due to precipitation of the reduction product. Results are shown in Table III. Since $i_{p,c}$ and $i_{p,a}$ values were so dissimilar, ΔE_p *vs.* i_p comparisons were not made. E_m-values were fairly independent of ν and are collected in Table IV.

The cation counterion in the Nafion affects the observed E_m-value for toluene reduction. The E° shift follows the series: $Li^+ > Na^+ > K^+$. This can be attributed to rapid ion

Table II. Cyclic voltammetric results for TCNQ in THF at the Pt-SPE electrode[a]

Nafion	ν	$E_{p,c}$	$E_{p,a}$	ΔE_p	E_m	$i_{p,c}$	$i_{p,a}$	$i_{p,c}/i_{p,a}$	$i_p/\nu^{1/2}$
Li^+	20	+148	+354	206	+251	48	36	1.3	11
	50	+95	+375	280	+235	84	70	1.2	12
	100	+50	+395	340	+220	92	82	1.1	9
Na^+	20	+145	+375	230	+260	38	44	0.9	9
	50	+110	+380	270	+245	65	68	1.0	9
	100	+60	+407	347	+234	87	90	1.0	9
K^+	20	+140	+338	198	+239	42	37	1.1	9
	50	+100	+348	248	+224	66	64	1.0	9
	100	+49	+371	322	+200	91	92	1.0	9

[a]As in Table I.

Table III. Cyclic voltammetric results for BQ in toluene at the Pt-SPE electrode[a]

Nafion	ν	$E_{p,c}$	$E_{p,a}$	ΔE_p	E_m	$i_{p,c}$	$i_{p,a}$	$i_{p,c}/i_{p,a}$	$i_{p,c}/\nu^{1/2}$
Li^+	20	−255	−164	109	−210	50	126	0.4	11
	50	−270	−137	133	−204	84	204	0.4	12
	100	−285	−110	175	−198	120	280	0.4	12
	200	−300	−80	220	−190	150	360	0.4	11
Na^+	20	−270	−180	0	−225	46	74	0.6	10
	50	−280	−168	112	−224	66	142	0.5	9
	100	−295	−145	150	−220	106	228	0.5	10
	200	−305	−140	165	−222	156	296	0.5	11
K^+	20	−310	−190	120	−250	56	130	0.4	12
	50	−330	−170	160	−250	90	200	0.4	12
	100	−340	−145	195	−242	136	260	0.5	13
	200	−365	−115	250	−240	212	388	0.6	15

[a]As in Table I.

Downloaded 02 Feb 2009 to 146.6.143.190. Redistribution subject to ECS license or copyright; see http://www.ecsdl.org/terms_use.jsp

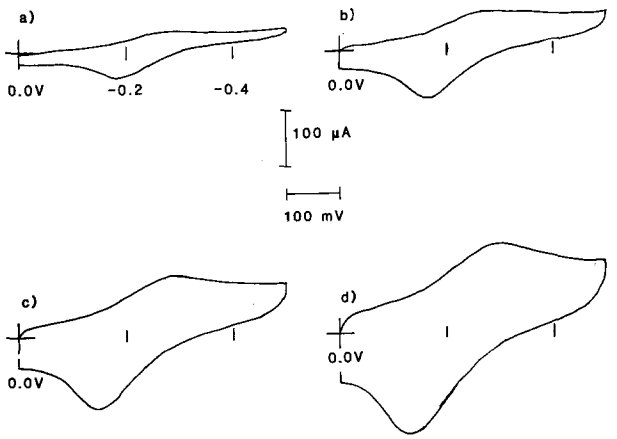

Fig. 11. Cyclic voltammetry of 10 mM BQ in $C_6H_5CH_3$ at a 1.98 × 10^{-2} cm^2 Pt-SPE electrode in the absence of added supporting electrolyte. Li^+ Nafion, all potentials in *V vs.* Ag/AgCl: (a) 20, (b) 50, (c) 100, (d) 200 mV/s.

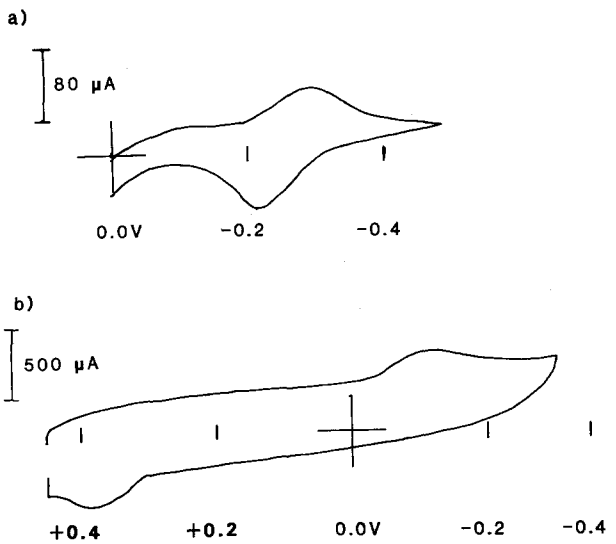

Fig. 12. Cyclic voltammetry of 10 mM TCNQ in $C_6H_5CH_3$ at a 1.98 × 10^{-2} cm^2 Pt-SPE electrode in the absence of added supporting electrolyte. All potentials in *V vs.* Ag/AgCl: (a) Li^+ Nafion, 50 mV/s; (b) Na^+ Nafion, 50 mV/s.

pair formation and precipitation between the radical anion and polymer cation. The electrochemical process can be considered as composed of two reactions, a reversible electron transfer followed by reversible and rapid precipitation

$$\text{Electron transfer } (E_r): \ BQ + e^- = BQ^- \ E^\circ_{BQ} \qquad [3]$$

$$\text{Precipitation } (C_r): \ BQ^- + M^+ = M^+ \ BQ^-(c) \ K_{sp} \qquad [4]$$

$$\text{Overall } (E_rC_r): \ BQ + e^- + M^+ = M^+ \ BQ^-(c) \ E^\circ_{M^+BQ} \qquad [5]$$

The formal potential of the E_rC_r reaction is

$$E^\circ_{M^+BQ} = E^\circ_{BQ} - (RT/F) \ln K_{sp} \qquad [6]$$

Therefore, the smaller the solubility product of the radical ion pair (K_{sp}), the more positive the potential for the overall reaction. The difference in formal potentials for the overall reaction ($E^\circ_{M^+BQ}$) is related to the ratio of K_{sp}'s as

$$E^\circ_{M^+BQ} - E^\circ_{Li^+BQ} = + (RT/F) \ln (K_{sp}^{Li^+}/K_{sp}^{M^+}) \qquad [7]$$

The relative magnitudes of the solubility products for radical ion salts of the M^+ ion with respect to that of the Li^+ ion for BQ in toluene are collected in Table IV. Generally an increase in the size of the cation ($Li^+ < Na^+ < K^+$) causes a decrease in the ion pair interaction ($Li^+ > Na^+ > K^+$) (29) and subsequent precipitation, in agreement with the observed electrochemical behavior.

Table IV. Relative ion pair strengths of alkali metal ions with the benzoquinone radical anion in toluene

Nafion form	E_m[a]	K_{sp}^{M+}/K_{sp}^{Li+}
Li^+	−200(±16)	1.00
Na^+	−223(±2)	2.45
K^+	−246(±5)	5.99

[a]All potentials in mV *vs.* Ag/AgCl.

The cyclic voltammetric behavior of TCNQ in toluene in the absence of supporting electrolyte is shown in Fig. 12; data are collected in Table V. In the presence of Li^+ counterions in the aqueous phase, Fig. 12a, the wave shapes are similar to those observed for BQ in THF and toluene, *i.e.*, a diffusion-controlled reduction and a symmetric, thin layer-like reoxidation. Values for $i_{p,c}/\nu^{1/2}$ were nearly constant, and $i_{p,c}/i_{p,a}$ ratios were 0.8-1.1. ΔE_p values, in the range 55-155 mV increased linearly with i_p, probably because of uncompensated resistance effects, but E_m remained constant at −0.26V *vs.* Ag/AgCl. In the presence of Na^+ counterions, the cyclic voltammetric behavior was significantly different (Fig. 12b). A solution of equal concentration of TCNQ yields peak currents three to four times larger (at comparable scan rates) than those observed in the presence of Li^+ counterions. The peak potentials of the reduction waves have moved to more positive values by *ca.* 0.2V, and the peak potentials of the anodic waves have shifted to more positive values by *ca.* 0.6V. Values for $i_{p,c}/\nu^{1/2}$ decreased with increasing scan rate, and ΔE_p values increased by eight-fold (at comparable scan rates) to *ca.* 400 mV. E_m was constant in the range of scan rates (5-50 mV/s) at +0.15V *vs.* Ag/AgCl. The observed behavior was reproducible for several trials with the Li^+ and Na^+ systems, suggesting a real chemical cause for the difference in behavior.

The apparently anomalous behavior for reduction of TCNQ in toluene in the presence of Na^+ in the membrane and aqueous phase can be explained by formation and precipitation of the conductive salt, Na^+ $TCNQ^-$ on reduction, and formation of solid TCNQ on the electrode surface on reoxidation. The large peak splitting and general nature of the CV behavior is similar to that found for the tetrathiafulvalene (TTF)-TCNQ system (30). The radical ion salts of these compounds can form segregated stacks of donor (TTF^+) and acceptor ($TCNQ^-$) molecules (31). The complex

Table V. Cyclic voltammetric results for TCNQ in toluene at the Pt-SPE electrode[a]

Nafion	ν	$E_{p,c}$	$E_{p,a}$	ΔE_p	E_m	$i_{p,c}$	$i_{p,a}$	$i_{p,c}/i_{p,a}$	$i_p/\nu^{1/2}$
Li^+	20	−280	−225	55	−252	44	40	1.1	10
	50	−290	−215	75	−252	74	88	0.8	10
	100	−315	−205	110	−260	110	121	0.9	11
	200	−340	−185	155	−262	163	162	1.0	12
Na^+	5	−25	+331	356	+153	106	108	1.0	47
	10	−55	+355	410	+150	148	132	1.1	47
	20	−50	+358	408	+154	160	130	1.2	36
	50	−125	+390	515	+132	200	202	1.1	28

[a]As in Table I.

Downloaded 02 Feb 2009 to 146.6.143.190. Redistribution subject to ECS license or copyright; see http://www.ecsdl.org/terms_use.jsp

interaction of forces that determine the structural arrangement has been a subject of several studies, but it is not completely understood for the alkali-metal salts of TCNQ (33). At room temperature and atmospheric pressure, Na^+ and K^+ salts of TCNQ (prepared from solutions of metal-iodide and TCNQ in MeCN) are found in a resistive, dimeric phase. When heated (33) or pressurized (34), these salts undergo a phase transition to a columnar infinite segregated stack structure of monomeric units, which is accompanied by a sudden increase in conductivity (33) and spin susceptibility (35). For Na^+ $TCNQ^{\cdot}$ at atmospheric pressure, the phase transition is continuous with an inflection point (transition temperature) at 72°C and a small (unobservable) heat of transition (33). The pressure-induced transition occurs in the range 135-175 kbar (32). Li^+ salts show behavior quite different from that of the other alkali metals and do not show a high temperature phase transition at atmospheric pressure (31-35). They also show an anomalous, low pressure phase transition near 10 kbar (32). A study of the dimerization of $Li^+TCNQ^{\cdot}$ salts in aqueous solutions found that, although the formation of dimers in water is highly favorable ($K = 2.5 \times 10^3$ liter/mol, $\Delta G^\circ = -4.6$ kcal/mol), no dimerization was detected in other protic and polar aprotic solvents of higher and lower dielectric constants than water (36). The investigators concluded that "specific solvation effects must be important in determining the stability of the dimer" (36). In toluene, Na^+ $TCNQ^{\cdot}$ salts could be electrocrystallizing into the columnar infinite segregated stack structure, due to solvent interactions which are great enough to overcome the small heat of phase transition. The formation of the conductive solid on the surface of the electrode increases the effective electrode area and results in increased peak currents in the presence of Na^+ compared with those with Li^+. Note that the buildup of $Na^+TCNQ^{\cdot}$ on the electrode surface probably increases continually with electrode cycling, because the TCNQ formed on reoxidation does not redissolve. TCNQ at the 10 m*M* concentration level is near the saturation limit, and TCNQ dissolves slowly and requires sonication. On repeated cycling the TCNQ concentration would build up near the electrode surface and only slowly dissolves. This would account for the peak current ratios near unity. Like the TTF system (30), the Na-TCNQ reaction may be thought of as a "square scheme" mechanism (37)

$$\begin{array}{ccc} \underline{TCNQ_A} + e^- + Na^+ & \rightarrow & \underline{Na^+TCNQ^{\cdot}_A} \\ \uparrow\ k & & \downarrow\ k' \\ \underline{TCNQ_B} + e^- + Na^+ & \leftarrow & \underline{Na^+TCNQ^{\cdot}_B} \end{array} \qquad [8]$$

The A forms have TCNQ-like structures and the B-forms stacked Na^+ $TCNQ^{\cdot}$ structures, with the structural rearrangements (k and k') being rapid and irreversible. The reduction of TCNQ in the presence of Na^+ ion occurs at a potential positive of its E° because of the following irreversible reaction (19d). The stabilization of the reduced form by formation of the stacked structure makes the stacked species harder to oxidize and shifts the oxidation wave to more positive potentials. The result is a cyclic voltammogram like that seen in Fig. 12b. The deposition of these electronically conducting salts on the platinum electrode surface increases the effective electrode area; resulting in the observed time-dependent increase in capacitive and faradaic currents at the Pt-SPE electrode. The formation of such conductive salt layers on thin Pt coatings may be useful in the preparation of modified SPE electrodes with special properties, *e.g.*, for promotion of electron transfer to enzymes (38).

Potential limits with different solvents.—The potential limits of the Pt-SPE electrode in all solvents with an unbuffered 1.0*M* LiCl counter solution are −1.3 to +1.2V *vs.* Ag/AgCl, as shown in Fig. 13. With a counter solution of 1.0*M* HCl, the cathodic limit was reduced to −0.2V *vs.* Ag/AgCl (Fig. 13b), while alkaline counter solutions did not increase the potential limits beyond those with an unbuffered, neutral counter solution. These data indicate that the cathodic limit of these Pt-SPE electrodes is probably governed by proton reduction. These protons are probably from residual water (1-2 H_2O/SO_3^-) in the membrane. A

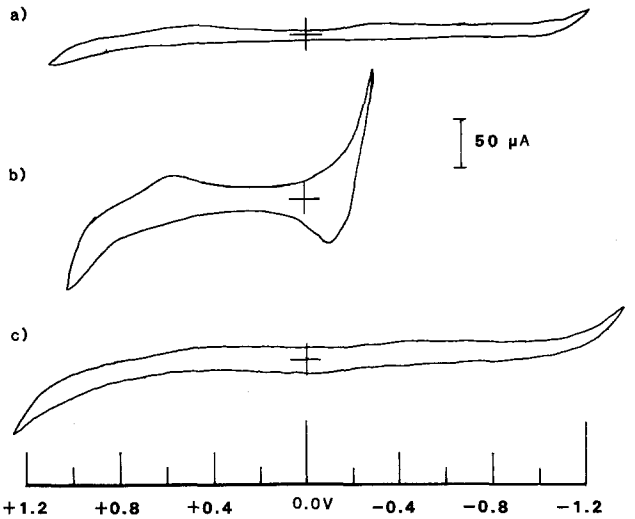

Fig. 13. Cyclic voltammetry of neat $C_6H_5CH_3$ at a 1.98×10^{-2} cm² Pt-SPE electrode. All potentials in *V* vs. Ag/AgCl: (a) 1.0M LiCl counter solution; (b) 1.0M HCl counter solution; (c) 1.0M TMACl counter solution.

well-defined amount of water, dependent on the cation, is retained in Nafion after vacuum drying, and is only desorbed after heating above the glass transition of the Nafion matrix (39). The energy of interaction between polymer and residual water is an estimated 15 kcal/mol^{-1} (39). Residual water probably remains in the ionic cluster site even after hydrophobic domains in the membrane have been penetrated and solvated by the nonaqueous working solution. In addition, water contacting the counter solution side of the membrane will resolvate the hydrophilic clusters and the cations that migrate from the counter solution are "aquated" and bring water to the nonaqueous solution/membrane interface. The use of aprotic counter solutions to extend the potential limits of these systems is currently under investigation.

Conclusions

Small area SPE-type electrodes have been shown to be useful for voltammetric investigations with highly resistive aqueous and nonaqueous solutions. The structure and electrochemical behavior of platinum electrodes supported on solid polymer electrolyte membranes was probed by scanning electron microscopy and cyclic voltammetry, respectively. The structure of the platinum electrode was found to be a thin (10-30 μm) layer on the surface of the supporting membrane. This thin layer was continuous, yet porous, necessary for both electronic conduction across the face of the electrode and ionic conduction through the membrane/electrode/solution interface. The electrochemical behavior suggested that electron transfer from the electrode to substrates in the working solution occur on the solution side of the electrode, not within the polymer matrix. The data also indicate that if the working solution is anhydrous and aprotic, the site of electron transfer is also anhydrous and aprotic. Large effective resistances are observed for electron transfer into aprotic media in the absence of supporting electrolyte. The kinetics of ion solvation into polar media may limit some processes. In apolar media, the electrochemistry is characterized by following chemical reactions, such as ion pair formation and precipitation.

Acknowledgment

The support of this research by the National Science Foundation grant no. CHE8402135 is gratefully acknowledged.

Manuscript submitted July 28, 1987; revised manuscript received Nov. 20, 1987.

The University of Texas at Austin assisted in meeting the publication costs of this article.

Downloaded 02 Feb 2009 to 146.6.143.190. Redistribution subject to ECS license or copyright; see http://www.ecsdl.org/terms_use.jsp

REFERENCES

1. See, *e.g.*, A. J. Appleby and E. B. Yeager, *Energy* (Oxford), **11,** 137 (1986) and references to earlier literature.
2. P. W. T. Lu and S. Srinivasan, *J. Appl. Electrochem.*, **9,** 269 (1979).
3. Y. Fujita, H. Nakamura, and T. Muto, *ibid.*, **16,** 935 (1986).
4. J. O. Howell and R. M. Wightman, *Anal. Chem.*, **56,** 524 (1984).
5. A. M. Bond, M. Fleischmann, and J. Robinson, *J. Electroanal. Chem. Interfacial Electrochem.*, **168,** 299 (1984).
6. (a) Z. Ogumi, K. Nishio, and S. Yoshizawa, *Electrochim. Acta,* **26,** 1779 (1981); (b) Z. Ogumi, H. Yamashita, K. Nishio, Z. Takehara, and S. Yoshizawa, *ibid.*, **28,** 1687 (1983); (c) Z. Ogumi, S. Osashi, and Z. Takehara, *ibid.*, **30,** 121 (1985).
7. (a) E. Raoult, J. Sarrazin, and A. Tallec, *J. Appl. Electrochem.*, **14,** 639 (1984); (b) E. Raoult, J. Sarrazin, and A. Tallec, *ibid.*, **15,** 85 (1985); (c) E. Raoult, J. Sarrazin, and A. Tallec, *J. Membr. Sci.*, **30,** 23 (1987).
8. (a) A. Katayama-Aramata and R. Ohnishi, *J. Am. Chem. Soc.*, **105,** 658 (1983); (b) A. Aramata and R. Ohnishi, *J. Electroanal. Chem. Interfacial Electrochem.*, **162,** 153 (1984); (c) A. Katayama-Aramata, H. Nakajima, K. Fujikawa, and H. Kita, *Electrochim. Acta,* **28,** 777 (1983).
9. H. Takenaka and H. Torikai, *Kokai Tokkyo Koho* (Japan Patent), **55,** 38934 (1980).
10. D. S. Acker and W. R. Hertler, *J. Am. Chem. Soc.*, **84,** 3370 (1962).
11. J. McBreen, *This Journal,* **132,** 1112 (1985).
12. G. G. Barna, S. N. Franks, and T. H. Teherani, *This Journal,* **129,** 743 (1982).
13. J. Bett, K. Kinoshita, K. Routsis, and P. Stonehart, *J. Catal.*, **29,** 160 (1973).
14. A. N. Frumkin, in "Advanced Electrochemistry," Vol. 3, P. Delahay, Editor, p. 287, John Wiley & Sons, Inc., New York (1967).
15. T. D. Gierke and W. Y. Hsu, in "Perfluorinated Ionomer Membranes," A. Eisenberg and H. L. Yeager, Editors, p. 283, ACS, Washington, DC (1982).
16. J. Lewin, *J. Am. Chem. Soc.*, **73,** 3906 (1951).
17. (a) M. Lopez, B. Kipling, and H. L. Yeager, *Anal. Chem.*, **49,** 629 (1977); (b) A. Lindheimer, J. Molenat, and C. Gavach, *J. Electroanal. Chem. Interfacial Electrochem.*, **216,** 71 (1987).
18. S. Mazur and S. Reich, *J. Phys. Chem.*, **90,** 1365 (1986).
19. A. J. Bard and L. R. Faulkner, "Electrochemical Methods," John Wiley & Sons, Inc., New York (1980) (a) pp. 699-700; (b) p. 218 (c) p. 521 and (d) p. 452.
20. L. E. Manring, *Polym. Comm.*, **28,** 68 (1987).
21. P. G. Galugla and H. Dirdi, *J. Membr. Sci.*, **25,** 311 (1986).
22. C. R. Martin, I. Rubinstein, and A. J. Bard, *J. Am. Chem. Soc.*, **104,** 4817 (1982).
23. L. R. Melby, R. J. Harder, W. R. Hertler, W. Mahler, R. E. Benson, and W. E. Mochel., *ibid.*, **84,** 3374 (1962).
24. R. Wheland and J. Gibson, *ibid.*, **98,** 3916 (1976).
25. H. Kita, K. Fujikawa, and H. Nakajima, *Electrochim Acta,* **29,** 1721 (1983).
26. G. Scibona, C. Fabiani, and B. Scuppa, *J. Membr. Sci.*, **16,** 37 (1983).
27. R. P. Buck, *ibid.*, **17,** 1 (1984).
28. M. Szwarc, in "Ions and Ion Pairs in Organic Reactions," Vol. 1, M. Szwarc, Editor, p. 1, John Wiley & Sons, Inc., New York (1972).
29. J. Smid, in "Ions and Ion Pairs in Organic Reactions," Vol. I, M. Szarc, Editor, p. 85, John Wiley & Sons, Inc., New York (1972).
30. T. P. Henning and A. J. Bard, *This Journal,* **103,** 613 (1983).
31. J. H. Perlstine, *Angew. Chem.*, (International English Edition), **16,** 519 (1977).
32. I. Shirotani and N. Sakai, *J. Solid-State Chem.*, **18,** 17 (1976).
33. J. G. Vegter, T. Hibma, and J. Kommandeur, *Chem. Phys. Lett.*, **3,** 427 (1969).
34. I. Shirotani, A. Ohodera, and N. Sakai, *Bull. Chem. Soc. Jpn.*, **48,** 167 (1975).
35. J. G. Vegter and J. Kommandeur, *Mol. Cryst. Liq. Cryst.*, **30,** 11 (1975).
36. R. H. Boyd and W. D. Phillips, *J. Chem. Phys.*, **43,** 2927 (1965).
37. P. J. Peerce and A. J. Bard, *J. Electroanal. Chem. Interfacial Electrochem.*, **114,** 89 (1980).
38. W. J. Albery, P. N. Bartlett, and D. H. Craston, *ibid.*, **194,** 223 (1985).
39. M. Escubes and M. Pineri, in "Perfluorinated Ionomer Membranes," A. Eisenberg and H. L. Yeager, Editors, p. 9, ACS, Washington, DC (1982).

Voltammetry at a Rotating and a Stationary Very Thin Ring Electrode

James S. Symanski*,[1] **and Stanley Bruckenstein***

Chemistry Department, State University of New York at Buffalo, Buffalo, New York 14214

ABSTRACT

A very thin ring electrode (VTRE) inlaid in an insulating glass plane has been fabricated and studied. Its inner radius was 4 mm and its width was 0.7 μm. Current-potential and current-time behavior for the reduction of ferricyanide in potassium chloride and iodine in excess iodide were studied at the rotating and the stationary very thin ring electrode. Comparison of the electrochemical data with theory indicated that the ring electrode was approximately 0.3 μm below the surface of the insulating plane. This conclusion was verified by means of scanning electron microscopy.

The rotating disk electrode (RDE) is one of the few electrochemical systems for which the hydrodynamic and convective-diffusion equations have been rigorously solved (1). It has been used widely in electrochemistry to study a great variety of electrochemical problems (2-5). Frumkin and Nekrasov (6) described the now familiar rotating ring-disk electrode (RRDE) which had a ring electrode concentrically surrounding the disk electrode. Subsequently, Ivanov and Levich (7) developed an approximate theory for collection experiments at the RRDE.

Zaidel (8) treated the problem of a separate rotating ring electrode (RRE) and derived the solution for the limiting convective-diffusion controlled current at such an electrode. It was shown that, unlike the RDE, the RRE does not possess the property of uniform accessibility. The mass flux to a RRE is infinite at the inner edge of the ring and decreases as the radial distance increases from the center of rotation. Moreover, the RRE was predicted to yield a larger mean current density than the RDE. The thinner the ring is, the higher is the theoretical mean current density. This property makes a thin ring electrode attractive for kinetic and analytical investigations. To test this conclusion, we have fabricated a rotating very thin

*Electrochemical Society Active Member.
[1]Present address: Johnson Controls, Incorporated, Corporate Applied Research Group, Milwaukee, Wisconsin 53201.

Downloaded 02 Feb 2009 to 146.6.143.190. Redistribution subject to ECS license or copyright; see http://www.ecsdl.org/terms_use.jsp